Title

Magic Numbers and Stabilities of Photoionized Water Clusters: Computational and Experimental Characterization of the Nanosolvated Hydronium Ion

Authors

Mackie, Cameron J
Lu, Wenchao
Liang, Jiashu
et al.

Peer reviewed

Magic Numbers and Stabilities of Photoionized Water Clusters: Computational and Experimental Characterization of the Nanosolvated Hydronium Ion

Cameron J. Mackie,[†,‡] Wenchao Lu,[†] Jiashu Liang,[‡] Oleg Kostko,[†] Biswajit Bandyopadhyay,[†] Ishan Gupta,[‡] Musahid Ahmed,[∗,†] and Martin Head-Gordon[∗,‡,†]

†*Chemical Sciences Division, Lawrence Berkeley National Laboratory, Berkeley, California 94720, USA*

‡*Department of Chemistry, University of California, Berkeley, California 94720, USA*

E-mail: mahmed@lbl.gov; mhg@cchem.berkeley.edu

Abstract

The stability and distributions of small water clusters generated in a supersonic beam expansion are interrogated by tunable vacuum ultraviolet radiation generated at a synchrotron. Time-of-flight mass spectrometry reveal enhanced population of various protonated water clusters $(H^+(H_2O)_n)$ based upon ionization energy and photoionization distance from source, suggesting there are "magic" numbers below the traditional $n = 21$ that predominates in the literature. These intensity distributions suggest that VUV threshold photoionization (11.0-11.5 eV) of neutral water clusters close to the nozzle exit leads to a different non-equilibrium state compared to a skimmed molecular beam. This results in the appearance of a new magic number at 14. Meta-dynamics conformer searches coupled with modern density functional calculations are used to identify the global minimum energy structures of protonated water clusters between $n = 2$ and 21, as well as the manifold of low-lying metastable minima. New lowest energy structures are reported for the cases of $n = 5, 6, 11, 12, 16, 18$, and special stability is identified by several measures. These theoretical results are in agreement with the experiments performed in this work, in that $n = 14$ is shown to exhibit additional stability, based on the computed second order stabilization energy relative to most cluster sizes, though not to the extent of the well known $n = 21$ cluster. Other cluster sizes that show some additional energetic stability are $n = 7, 9, 12, 17, 19$. To gain insight into the balance between ion-water interactions and water-water interactions as a function of cluster size, an analysis of the effective 2-body interactions (which sum exactly to the total interaction energy) was performed. This analysis reveals a cross-over as a function of cluster size between a water-hydronium dominated regime for small clusters and a water-water dominated regime for larger clusters around $n = 17$.

Introduction

The unquestioned importance of water in biological[1] and atmospheric[2] processes on Earth and in astrochemistry,[3] drives our quest to study the photon-induced dynamics of hydrogen

bonded water clusters at the molecular level.[4] The process through which water clusters form under various conditions is hence critical to understand. The growth of water clusters from molecular constituents has been a topic of active discussion since the inception of molecular beams and supersonic jets. Indeed, Searcy and Fenn[5] reported in 1974, the presence of magic numbers in protonated water clusters, n=21 being predominant among the distribution. Subsequently there has been additional experimental and theoretical work (reviewed below) seeking to understand the structure and stability of small water clusters. For example, Hansen et al. using an electrospray ionization source have observed magic numbers of $n = 4$ and 55 in water clusters besides $n = 21$, and a magic number of $n = 28$ in their deuterated water cluster experiments.[6,7] They have also investigated the mass spectrometric abundance and the dissociation energies of clusters up to $n = 120$, and proposed that the $n = 21$ protonated water cluster shows specific typological stability due to a shell closure, whereas the other minor magic numbers occur only because of the instability of the $n + 1$ precursor.[6] In addition, Lengyel et al. using electron impact ionization have indicated a possible magic number of $n = 10$.[8] These examples from the literature illustrate that the coupling of supersonic molecular beams to ionization sources allows for mass spectrometry, however the analysis of the results can be complicated. The pressure of the gas, and the temperature of the nozzle can have dramatic influence on the resulting cluster distribution. This arises due to the collisions between the gas molecules and the resulting drop in density and lowering of translational/vibrational-rotational energies that leads to cluster formation. This neutral cluster distribution is also affected by fragmentation that occurs upon ionization for mass spectrometry. Hence the final distribution observed is a convolution of the conditions of the supersonic expansion with that of the dynamics of ionization. The practice of Infrared (IR) spectroscopy to analyze mass-selected cluster ions coupled with detailed electronic structure calculations of the vibrational spectra has become the method of choice to alleviate these complications.

Over the last two decades, there have been precise reports of IR spectroscopy of size

selected protonated water clusters from the laboratories of Johnson, Duncan and Fujii[9–11] Recently, the implementation of VUV photoionization coupled to IR spectroscopy from a Free Electron Laser generated spectra for small neutral water clusters at an unprecedented level of detail,[12–14] This complements and extends early work pioneered by Buck and Huisken whose spectroscopic investigation of size-selected neutral clusters set the stage for these kinds of investigations.[15] Work by Buck et al.[16,17] has focused on using IR spectroscopy on large water clusters detected in mass spectrometry by sodium ion doping, to provide constraints for the temperature evolution from the nozzle to cluster detection in the mass spectrometer. The FEL experiments are unique, in that with VUV photoionization performed at threshold, leads to less fragmentation compared to electron impact and chromophore-based ionization hence allowing for a more definitive detection of the structure of small neutral water clusters. These results complement earlier work seeking to understand the unique characteristics of protonated water clusters, particularly for $H^+(H_2O)_{21}$, and to trace a pathway for the structure of the water clusters as they increase in size.[18] Beyond IR spectroscopy, there have been efforts to understand the hydrogen bond network of ionized water clusters using the tools of supersonic molecular beam mass spectrometry coupled with VUV single photon ionization,[19–21] multiphoton ionization,[22] electron impact ionization,[8,23,24] and by sodium ion tagging.[24] All of these methods lead to the formation of protonated water clusters. However, it has been shown that under various conditions of cooling, and upon threshold ionization, non-protonated ionized water clusters can be generated via a process of excitonic transfer from Ar* to core water clusters,[25] which was not observed in electron impact ionization.[23] Misuke et al.[26] also performed IR spectroscopy on these systems to show that the non-protonated water clusters contained a $H^+(H_2O)_n \cdot OH$ motif, where the OH radical was retained within the water cluster network. However, to date, there remain gaps in understanding the difference in the hydrogen bond network between neutral and protonated clusters as they evolve in size towards the bulk, as most studies have focused on the particularly stable n=21 cluster.

Turning to computational research, the rich variety of low-energy isomeric structures of protonated water clusters poses a predictive challenge whose difficulty rises approximately exponentially with the size of the cluster. Early work through 1997 has been reviewed,[27] and further progress through 2005 was summarized in a subsequent review,[28] that also included experimental work. Benchmarking studies on smaller protonated water clusters have also been performed in order to characterize the importance of many-body effects, as well as to assess the performance of density functional methods for capturing such effects.[29–31] A number of studies have been performed focusing on small cluster sizes illustrating the delicate interplay of factors determining the lowest free energy structure. Readers may consult Fig. S3 to see images of the competing low-energy structures that we review next. The protonated pentamer was controversial,[32] with the present picture favoring a branched structure.[33] Theoretical work on $H^+(H_2O)_6$ addressed the question of whether the lowest energy conformer is a branched structure or a cyclic ring structure. The final determination (branched) required treatment of electron correlation effects (at the MP2 level) and also anharmonic zero point vibrational energy (ZPVE) corrections.[34] Subsequent experimental work (corroborated by theory), suggested that two branched isomers co-exist.[35] Similar computational refinement was needed for $H^+(H_2O)_7$ clusters in order to determine whether the lowest energy conformer is a ring structure as suggested by experiment, or a closed structure.[36] The overall takeaway, perhaps unsurprising, is that adequate treatment of electronic structure and nuclear quantum effects are both required to fully resolve the stability of even these relatively small water clusters.

Beyond $n = 7$, thorough enumeration of the isomers (and thus global minimum searches) of individual cluster sizes becomes increasingly challenging; the number of low energy conformers increases rapidly and the energy gap between the different conformers closes. Coupled to this is the unfavorable size-scaling of both benchmark-level electronic structure calculations, as well as anharmonic vibrational calculations (or path integral molecular dynamics). Even including harmonic ZPVE corrections, the ordering of the lowest energy conformers

can change with the basis set or methods used (ZPVE, etc.);[37] even so far as to favor open structures over caged structures for certain cluster sizes (for examples, see Figs. S3 and S4). The level of theory described above (adequate treatment of electron correlation and anharmonic ZPVE) to settle questions about $n \leq 7$ rapidly become unfeasible for larger cluster sizes (although transferable machine-learned potentials may offer promise[38]).

An important prerequisite to fully resolving the temperature-dependent lowest free energy conformer of the larger water clusters is to identify the lowest electronic energy structures at a reliable yet affordable level of theory, as well as all competing low-energy structures. To do so, sophisticated efforts using search methods such as basin-hopping have been performed up to the size range of $n \sim 21$.[39–41] These studies have characterized some general trends in preferred isomer as a function of cluster size. Examples include the relative stability of large and smaller clusters with respect to gain or loss of a water molecule, the location of the hydronium cation (always on the surface), and occurrence (or lack) of a fully solvated ("core") H_2O beyond $n = 16$, and the general progression of growth (from branched, to ring, to cage, to solvated H_2O). Minimum energy structures from reference 39 are available for $n \leq 21$. These minima were obtained using two different empirical potentials: one by Kozack and Jordan (KJ),[42] and the other developed by the authors, called the anisotropic site potential (ASP).[43] Reference 41 uses an energy-based "comprehensive genetic algorithm" (CGA)[44] to investigate $n = 10 - 17$. Unfortunately, the optimized geometries of reference 41 are not available, however the authors included comparisons to the KJ and ASP energies of reference 39, as well as graphical representations of their structures, such that comparisons of lower energy conformers can be inferred.

The $H^+(H_2O)_{21}$ cluster has received dedicated computational study due to its observed magic nature in experiments, and as such its PES and infrared spectrum have been studied more than the surrounding cluster sizes.[45–47] Experiment and theory agree that the hydronium ion remains on the surface, with a fully solvated H_2O molecule in the center. The theoretical explanation of the source of stability of this magic number remains unsettled,

although many hypothesis have been put forth, including geometric arguments of highly symmetric pentagonal-dodecahedron-like structures for $n = 21$.[48]

In this work, we seek to understand the structural evolution of small protonated water clusters with size by changing the source conditions (backing pressure, nozzle to ionization distance, and photon energy) in the experiment and performing electronic structure theory calculations. The intensity distributions and internal temperature of clusters in continuous supersonic jets are typically controlled by varying the initial conditions (backing pressure and temperature) and using nozzles of different sizes[49,50] while in pulsed beams, varying the timing between the expanding gas and the laser (or an electron gun) leads to control of internal temperatures.[51–54] We have chosen to use a synchrotron-based mass spectrometry technique in which a continuous supersonic beam is ionized at different axial distances from the nozzle to sample various regimes of the supersonic expansion.[55–57] The distribution at each distance is a result of the non-equilibrium processes during the formation and growth of these clusters. Using this method, we have generated protonated water cluster distributions as a function of photon energy (controls internal energy) and nozzle to ionization distance (controls temperature and ionization dynamics). The internal energy of a photoionized molecule depends on the difference between its adiabatic ionization energy and the photon energy that is used to ionize the molecule. While there is speculation that the departing electron does remove some of the energy,[20] and evaporation of both Ar (carrier gas) and water can also dissipate this internal energy, we[58] and others have shown that internal energy can give rise to fragmentation. Mass spectral distributions and photoionization intensity curves have been particularly useful for depicting fragmentation mechanisms, structural rearrangements and ion-molecule reactions.

Ab-Initio molecular dynamics processes can provide clarity and detail in the ionization processes that occur upon ionization of both water clusters and in the bulk.[59–61] The ionization of the water from the highest occupied molecular orbital (HOMO) produces a water radical cation ($H_2O^{+\bullet}$) and a proton is transferred to the neighboring water molecule forming

7

hydronium ion (H_3O^+) and OH$^\bullet$ radical:

$$H_2O^{+\bullet} + H_2O \longrightarrow H_3O^+ + OH^\bullet \tag{1}$$

The ionization of larger clusters similarly undergo rapid proton transfer and fragmentation to produce protonated water clusters of the form $H^+(H_2O)_n$.

$$(H_2O)_n + h\nu \longrightarrow (H_2O)_n{}^{+\bullet} + e^- \longrightarrow H^+(H_2O)_{n-1} + OH^\bullet + e^- \tag{2}$$
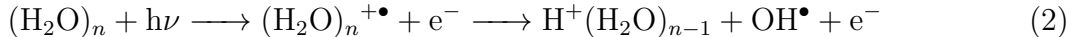
Reaction 2 produces protonated clusters regardless of the ionization conditions (photoionization or electron ionization). Thus vacuum ultraviolet photoionization experiments generate hydronium ions solvated in water clusters; the new experimental data presented here suggests that there is special stability associated with the $H^+(H_2O)_{14}$ cluster, in addition to the well-known special stability of $n = 21$.

To complement the experimental results, we also present results from electronic structure theory-based computational searches for the global minimum energy structure for $H^+(H_2O)_n$ clusters ranging from $n = 2 - 21$ (as well as all competing low-energy structures that we can identify). Our work employs more reliable levels of electronic structure theory than previous efforts to characterize such structures, and includes extensive conformational characterization for all cluster sizes. Specifically, we use a density functional (ωB97M-7[62]) that performs statistically better than those used earlier (B97-D and B3LYP) for non-bonded interactions.[63,64] Zero point energy corrections are included, at the harmonic level.[65] The relative stability, or "magic", of the resulting lowest energy conformers is then compared against neighboring cluster sizes through a number of measures including the sequential interaction energy, the second-order difference energy, and the interaction energy per molecule, as defined in the Computational Methods section. In each case, these measures can be compared to the well established magic number of $n = 21$. Additionally, some comparisons are made to theoretical results of neutral water clusters in order to provide perspective on the

behavior of the protonated water clusters.

Experimental Methods

The experiments are carried out in a continuous supersonic expansion chamber coupled to a three-meter vacuum ultraviolet (VUV) monochromator on the Chemical Dynamics Beamline (9.0.2), located at the Advanced Light Source, Berkeley, California. The experimental setup has been described previously.[55–57] In brief, 400 – 500 Torr of argon with seeded water vapor was expanded through a 100 μm nozzle to a differentially pumped chamber which was kept at a pressure of 2×10^{-4} Torr. The beam was intersected by the VUV radiation at various axial distances from the nozzle (2, 6, 10, 15, 20, 25, 30 mm), and the resulting ions were sampled into a reflectron time-of-flight (TOF) mass spectrometer. The ionization distance is varied by changing the nozzle position with respect to the point of intersection of molecular and VUV beams. A set of four electrodes were used to guide the ions from the ionization region to the mass spectrometer through a skimmer. The lenses were kept at small potentials (+5, 0, -3, and 0 V, respectively) and the skimmer is grounded. The TOF chamber of the mass spectrometer was kept at 2×10^{-6} Torr. A start pulse for the TOF was provided by pulsing the repeller and accelerator plates because of the quasi-continuous (500 MHz) nature of the synchrotron light. The ions were pulse-extracted by fast switching of repeller and accelerator plates to 1100 V using a pulse width of 7.0 μs. Ions were accelerated perpendicularly to their initial flight path through the field-free region and detected by a microchannel plate (MCP) detector that is installed at the end of the flight tube. Mass spectrometer settings were kept fixed while the ionization distance is varied. The time-dependent electrical signal from the detector was amplified by a fast preamplifier, collected by a multichannel scalar card, and then integrated with a computer. TOF spectra were measured at different positions in the photon energy range between 10 and 14 eV. The photoionization intensity curves were obtained by integrating peak intensities at each photon energy with a step size of 0.1 eV and

9

normalized by the photon flux.

Computational Methods

The conformer search of protonated water clusters $(\mathrm{H}^+(\mathrm{H_2O})_n)$, ranging in size from $n = 2$ to $n = 22$, was performed using the CREST[66] driver program for the density functional extended tight-binding (xTB) method.[67] The meta-dynamics used in the conformer search are carried out using the included iMTD-sMTD routines, which in addition to the standard meta-dynamics conformer search, also includes nondynamical steps, akin to basin hopping procedures.[66,68,69] The default settings for the iMTD-sMTD routine are used, which includes dynamically determining the optimal values for the simulation parameters; see reference 66 for more details. The only default setting changed is the optimization of the final conformer structures, which is set to "extreme" (an energy convergence of 5×10^{-8} E_h, and gradient convergence of 5×10^{-5} $\mathrm{E}_h a_0^{-1}$). This tight geometry optimization was performed to reduce compute costs for the subsequent density functional theory (DFT) optimizations, as GFN2–xTB[70] methods can provide quite good starting geometry guesses at low computational cost. The lowest energy $\mathrm{H}^+(\mathrm{H_2O})_{22}$ conformer is included in order to allow for the computation of $\Delta_2 E(21)$.

Conformers within 6 kcal/mol of the lowest energy structure of each cluster size were retained for refinement. Possible duplicates are flagged by their energies, dipole moments, and moments of inertia; and manually verified and removed. Geometry optimizations, harmonic frequency calculations at optimized geometries, and large basis single point calculations were then performed using accurate hybrid density functional theory (DFT) on the retained conformers. These DFT calculations were performed with a development version of the Q-Chem 5.4 program,[71] utilizing a newly developed analytical frequency capability[65] for VV10-containing functionals.[72] The geometry optimization and ZPVE calculation were carried out at the ωB97X-V[73]/def2-SVPD[74,75] level of theory, while the single point calcu-

lations are carried out at the ωB97M-V[62]/def2-TZVPPD[74,75] level of theory. This level of theory has proved to be quite accurate for non-bonded interactions based on a broad range of benchmarks.[63,64] As an additional comparison, our DFT results up to $n = 15$ are also compared against MP2 single-point energies using the aug-cc-pVTZ basis set; as shown in Figure 1 the sequential interaction energies are in very good agreement. This is a meaningful comparison because MP2 is known to be quite successful[76] for water[77–79] and ion-water clusters[80,81] (despite the fact that it needs refinement to be useful more broadly[82]). Reference 31 also benchmarked a number of density functionals against complete basis set limit of CCSD(T) reference data for $n \leq 5$ and found ωB97M-V to be the most accurate. All resulting conformers can be found in the Supplemental Material.
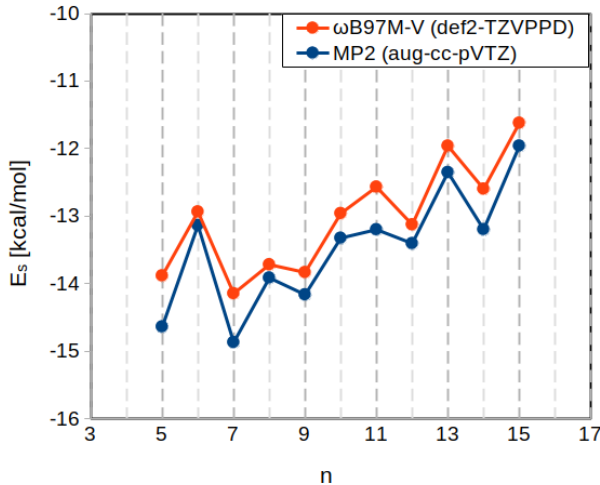

Figure 1: The sequential interaction energies (kcal/mol) of $H^+(H_2O)_n$ calculated with the ωB97M-V functional and def2-TZVPPD basis (orange), benchmarked against the MP2 energies calculated with the aug-cc-pVTZ basis, showing good qualitative agreement.

As already discussed, there are three main existing sets of conformer searches on protonated water clusters.[39,41] Therefore, when available, the geometries of lowest energy conformers of these previous studies were also refined using the same computational protocol discussed above. Both the "KJ" and "ASP" structures from reference 39 are included in this comparison. Since the geometries from reference 41 are not available, only topological comparisons and comparisons relative to the KJ and ASP energies can be made. Geometries

of the lowest energy structures of the neutral water clusters were obtained from reference 40, and we have re-evaluated the structures and relative energies at the same level of theory as we employ for the protonated clusters.

Multiple measures of the stability of a particular cluster size, $H^+(H_2O)_n$, relative to other cluster sizes (i.e., the degree of "magic"), have been proposed. The sequential interaction energy, $E_s(n)$, is given by

$$E_s(n) = E_I(n) - E_I(n-1), \tag{3}$$

where the interaction energy, $E_I(n)$, is defined as

$$E_I(n) = E(n) - \sum_{i=1}^{n} E_i, \tag{4}$$

where E_i are the energies of the relaxed isolated monomers of the cluster (with hydronium being considered a cluster). We see that $E_s(n)$ measures the increment in binding energy due to addition of the nth water molecule: if this is large and negative there is special stability.

The second-order difference energy is given by

$$\Delta_2 E(n) = 2E(n) - E(n-1) - E(n+1) \tag{5}$$

By contrast with the sequential interaction energy, $\Delta_2 E(n)$ assesses twice the interaction energy of the n-mer against the sum of interaction energies of the $(n-1)$ and $(n+1)$-mers. Such a double comparison makes particularly stable clusters more evident as negative-going peaks in plots of $\Delta_2 E(n)$ vs n.

The many-body expansion (MBE) has been widely used to understand cooperative effects in systems such as water clusters.[83–88] The effective 2-body interaction energy,[89] $\Delta E_{AB}^{\text{eff}}$, between 2 tagged molecules in a complex n-body system has been recently defined such that the MBE terminates *exactly* at the 2-body term, rather than the n-body term. In other

words:

$$E_{\text{tot}} = \sum_i^n E_i + \sum_{i<j}^n \Delta E_{ij}^{\text{eff}} \qquad (6)$$

To P-th order in the MBE, $\Delta E_{AB}^{\text{eff}}$ may be evaluated as:

$$\Delta E_{AB}^{\text{eff}}(P) = \sum_{p=2}^{P} \frac{2}{p(p-1)} \sum_{k_1<k_2<...<k_{(p-2)}\neq A,B} \Delta E_{ABk_1k_2\cdots k_{(p-2)}} \qquad (7)$$

where $\Delta E_{ABk_1k_2\cdots k_{(p-2)}}$ is the conventional P-th order many-body interaction energy.[89] $\Delta E_{AB}^{\text{eff}}(P)$ can be used to examine the pairwise interaction of any two bodies within the system, taking the cooperativity of the full system into account. In this work $P = 4$ is used, using the recursion formula given by equation 13 in reference 89. This means the interaction energies up to four-bodies are exact, with the remaining $p > 4$ n-body interaction energies slightly overestimated ($\sim$0.1 kJ/mol per interaction; see reference 89 for full details and benchmarking of errors). The full set of effective 2-body interactions defines the environment-dependent values of each hydronium-water interaction in each cluster, whose distribution can then be compared and contrasted against the corresponding distribution of water-water interaction energies.

Experimental Results

The mass spectra of water clusters at various nozzle-to-ionization distances (expansion distances) of 2, 6, 10, 15, 20, 25, and 30 mm were recorded with the range of ionization photon energy from 11.0, 11.3, 11.5, 11.7, 12.0, 12.5, 13.0 and 13.5 eV. The most important results are presented in Figure 2 and summarized in Figure S1. At the shortest nozzle to ionization distances (2 and 6 mm), strong intensity at $H^+(H_2O)_{14}$ is observed together with the typically observed "magic number" at $H^+(H_2O)_{21}$ which dominates at higher photon energy and longer nozzle to ionization distance. Beyond 14, and 21, there are other cluster sizes which also deviate from linearity in their mass spectral intensity, particularly above the 12.0
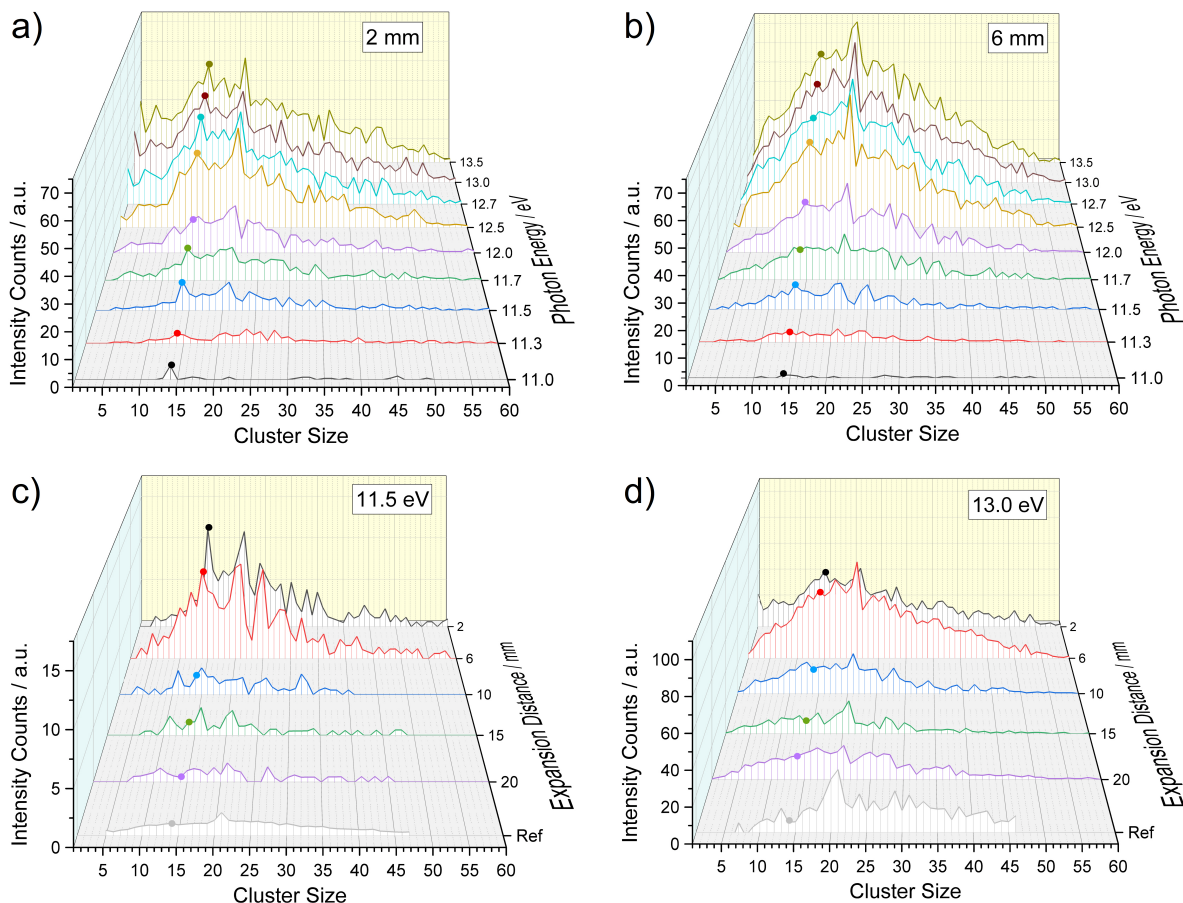
Figure 2: The intensity distribution of protonated water clusters $H^+(H_2O)_n$ as a function of photon energy at (a) 2-mm and (b) 6-mm expansion distance before ionization; and as a function of expansion distance before ionization at (c) 11.5 and (d) 13.0 eV. The gray thick lines are the data extracted from the results of Belau et al.[21] performed on a skimmed molecular beam. The highlighted dots of each spectrum indicate the magic numbers $n = 14$. See Fig. S1 for a full presentation of all data.
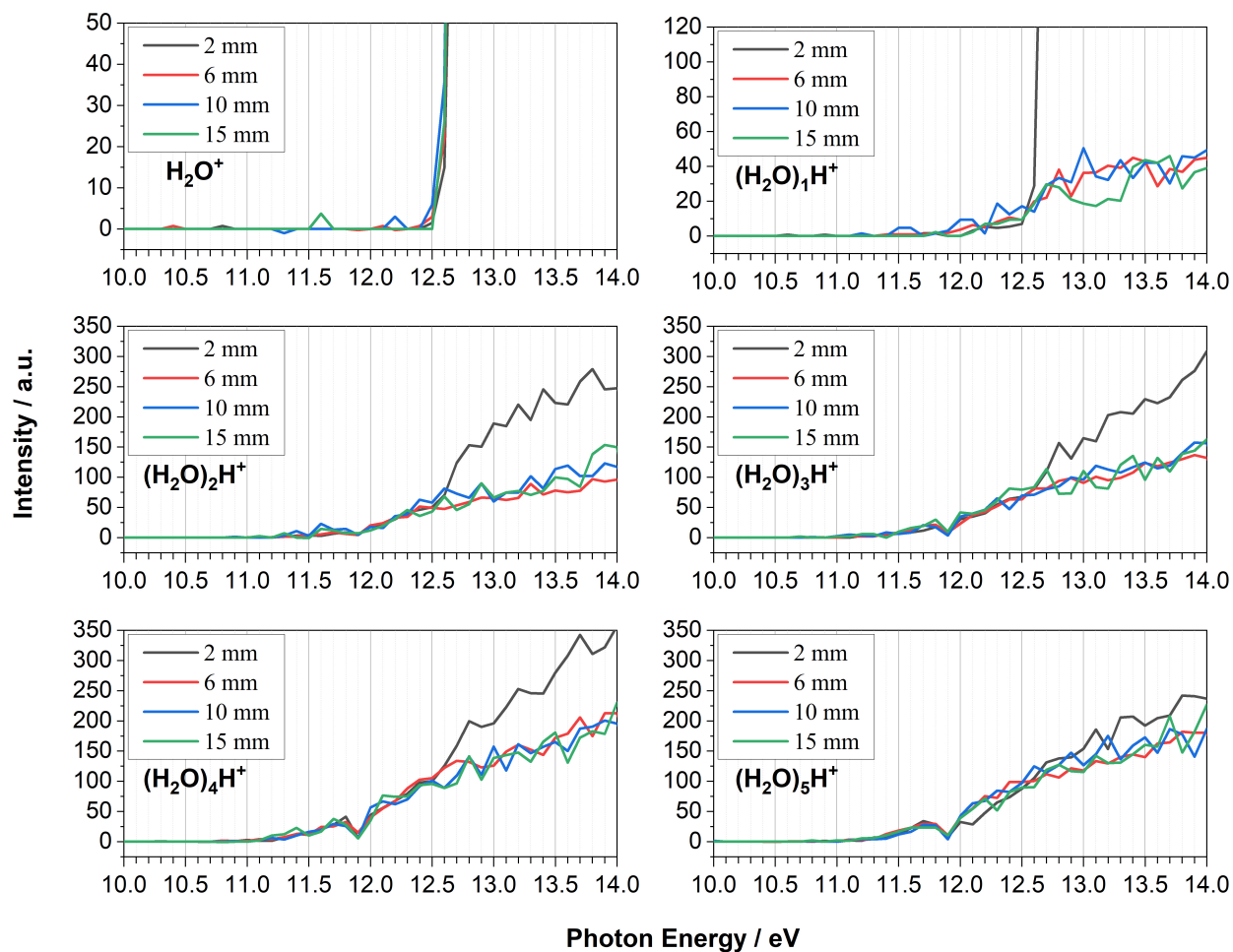
Figure 3: Photoionization intensity curves measured for water monomer and protonated water clusters ($H^+(H_2O)_n$ $n = 0$ to 5) at four different nozzle to ionization distances (2, 6, 10 and 15 mm). The dip in the spectra around 11.9 eV is due to absorption of an argon resonance from the gas filter used to remove higher harmonic radiation from the synchrotron. See Fig. S2 for a full list from $n = 0$ to 21.

eV ionization energy threshold. $n = 11$ is particularly prominent, while to a lesser extent, enhancement is also seen for $n = 16$ and $n = 19$. This can be seen directly in Figure 2. Here the intensities of the mass spectra between n= 7 to n=22, are displayed as a function of nozzle to ionization distance (2, 6, 10, and 15 mm). Overall, while $n = 21$ and $n = 14$ dominates as a magic number, $n = 11, 16$ and 19 also show enhanced stability. The overall mass spectra shows an envelope up to $n = 60$, with intensities rapidly decreasing after 10 mm ionization distance. In comparison, the reference curves in Figure 2(c) and (d) are from the results of Belau et al.[21] where ionization was performed after the skimmer, and corroborates that with the nozzle to ionization distance of 20 mm, only the $n = 21$ magic number dominates.

Our recent study of the growth of methanol clusters using the same experimental scheme will guide our explanation of the trends observed here.[55] The cluster distributions and photoionization intensity curves for methanol clusters showed that depending on the ionization distance, either the protonated methanol trimer or the dimer was the most stable ion. During a supersonic expansion, most collisions happen right at the exit of the nozzle and cluster formation occurs within 10-20 nozzle diameters.[90] Closer to the exit, the density of gases is also higher and calculations using a continuum model suggest that it drops to ~1-2% after 20 nozzle diameters. Since we have used a 100 μm nozzle, we expect maximum clustering to occur within 1-2 mm from the exit of the nozzle. Closer to the nozzle and above the ionization energy (12.6 eV), water readily forms H_2O^+ cation which initiates a reaction with another water to form hydronium ion and OH radical (reaction 1). After the initial formation of hydronium ion, neutral water molecules would condense around it to form protonated water clusters. It is also possible that the neutral clusters formed during the expansion get ionized followed by proton transfer and fragmentation to produce protonated water clusters (reaction 2). As the distance increases, the density diminishes for both water monomer and clusters, and ionization of neutral clusters are more probable farther from the exit due to the absence of ion-molecule collisions.

This hypothesis can be confirmed by tracking the photoionization intensity curves of protonated water clusters as a function of nozzle to skimmer distance. Figure 3 displays photoionization intensity curves for protonated water clusters for the monomer, and $H^+(H_2O)_n$ ($n = 0$ to 5) for four (2, 6, 10 and 15 mm) nozzle to ionization distances. At all measured distances, the appearance of the water monomer occurs at 12.61 eV confirming that it is indeed the neutral water monomer that is being ionized in the expansion. The protonated monomer at 2 mm is formed from a H_2O^+ cation while it would appear that at other distances, this arises at around 11.78 eV, which sits close to the ionization of a neutral water dimer. On examination of the AE's for $H^+(H_2O)_n$ ($n = 2, 3, 4$), it would suggest that at 2 mm, it is indeed ion molecule collisions, between an ionized monomer with neutral water clusters, that is giving rise to the intensity (reaction 1) while the residual signal arises from ionization from neutral water clusters. Beyond this, all appearance energies and shape of the photoionization intensity curve converges to ionization from neutral water clusters. Note that the appearance energies and photoionization intensity for $n = 14$ and 21, the magic numbers, show exactly the same properties as other clusters near its vicinity. Based on this analysis, it would appear that contribution from ion induced nucleation only occurs for protonated water clusters only up to $n = 4$ at 2 mm nozzle to ionization distance, or at least is observable in our experiment. Hence the enhancement of $n = 14$ observed in our experiment is not dependent on ion molecule collisions, but arises from metastable decay and evaporation upon photoionization of neutral water clusters. As shown earlier in the mass spectra in Figure 2(c) and (d), we compare results from photoionization of a supersonically skimmed water cluster beam at the same ionization energies (11.5 and 13.0 eV). This cluster distribution which shows only the magic number at 21, is a thermally equilibrated system. In contrast, the strong presence of $n = 14$ in photoionization at short nozzle to ionization distances will arise from the strongly non equilibrium conditions within a highly dynamic collision environment. We hypothesize that the absence of $n = 14$ in more "traditional" ionization studies arises from an annealed distribution which has frozen out in the distance it

has traveled from the nozzle to ionization. We now turn to theory to explore the comparative stability of $n = 14$ relative to other clusters, to shed light on this interesting experimental result.

Computational Results

Conformer search

We begin with an overview of the results. Figure 4 displays the geometries of the lowest energy conformers for each cluster size. The oxygen of the hydronium cation is colored blue in order to assist the reader in determining its location. As the cluster size increases, so do the number of arrangements of the hydrogen bond network, and therefore the gaps to higher energy structures are often very small: competitive low-energy conformers (within 1 kcal/mol) are shown in Figs. S3 ($n = 5 - 8$), S4 ($n = 8 - 11$), S5 ($n = 12 - 16$), and S6 ($n = 17 - 21$). Table 1 lists the total binding energies of the lowest energy conformers of this work, as well as the energies relative to the KJ and ASP structures[39] optimized at the same level of theory, and the number of structures that lie within 1 kcal/mol, and between 1 and 2 kcal/mol of the global minimum for each cluster size.

Energetically, all structures resulting from our conformer searches are found to be equivalent to or lower in energy than the KJ and ASP structures. Energetically and topologically, our optimized structures for $n = 2, 3, 4, 7$ can be considered equivalent to both of the (reoptimized) KJ and ASP structures. Considering now only the lowest energy structure of the KJ and ASP pair, we consider our optimized structures to be equivalent for the following cases: $n = 8$ (KJ), 9 (ASP), 13 (KJ), 19 (ASP), 20 (ASP), and 21 (ASP). This leaves the cases where our searches identified new candidates as global minima. Specifically, for $n = 5, 6, 10, 11, 12, 14, 15, 16, 17, 18$ the conformers of this work were found to be lower in energy than both the best candidates from KJ and ASP (after reoptimization).

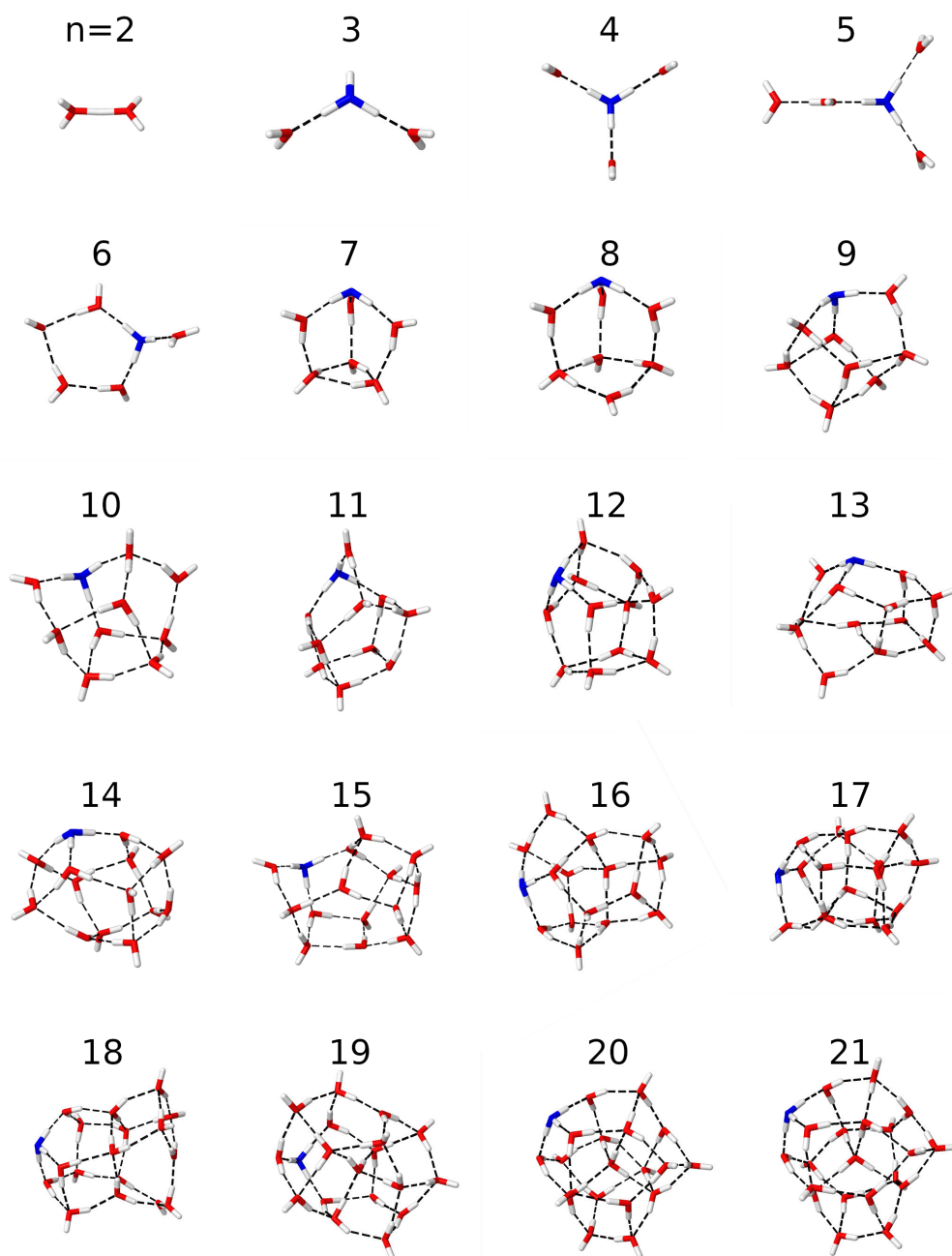Although no raw geometries are available for the Shi dataset[41] ($n = 10 - 17$), comparisons

Figure 4: The lowest energy conformers of the protonated water cluster, ranging in size from $n = 2$ to 21. The oxygen of the hydronium ion is colored blue to ease identification.

Table 1: The total interaction energies, E_I (kcal/mol; Eq. 4) of the lowest energy conformers optimized in this work (ZPVE correction included). The optimization and ZPVE calculation were carried out at the ωB97X-V/def2-SVPD level of theory, while the single point calculations were performed at the ωB97M-V/def2-TZVPPD level. Also listed are the binding energies of the KJ and ASP conformers relative to geometries found in the search performed in this work (ΔE(X) = E(Current search) - E(X)), after reoptimization and single point energy evaluation at the same level of theory used here (ZPVE correction included). The last two columns report the number of conformers found within 1 kcal/mol, and between 1 and 2 kcal/mol of the minimum energy conformers respectively.

$H^+(H_2O)_n$	E_I [kcal/mol]	ΔE(KJ)	ΔE(ASP)	# < 1 kcal/mol	1 < # < 2 kcal/mol
2	-34.17	-0.05	0.02	1	0
3	-54.34	0.01	0.00	1	0
4	-66.32	0.00	0.01	1	0
5	-83.07	-0.87	-0.91	3	0
6	-93.39	-1.36	-2.20	6	1
7	-103.70	-0.04	-0.04	9	5
8	-115.13	-0.02	-2.49	2	6
9	-125.02	-0.83	-0.01	5	4
10	-135.77	0.02	0.03	4	2
11	-145.67	-1.95	-0.07	6	13
12	-155.83	-1.45	-0.95	2	8
13	-165.78	0.01	-0.16	2	2
14	-175.54	-1.48	-1.51	3	2
15	-184.35	-2.57	-1.35	2	0
16	-194.98	-2.24	-0.48	2	1
17	-204.21	-1.07	-0.82	2	1
18	-214.22	-2.56	-0.04	3	0
19	-225.26	-1.38	-0.03	1	2
20	-234.38	-0.04	-0.09	4	1
21	-247.03	-0.04	-0.10	2	0

to this work can be made using the topologies (2D visualizations) they provide in their supplemental material, along with the aid of their comparisons to the KJ and ASP energies (re-optimized at their level of theory; B97-D/aug-cc-pVDZ). Based on this, for the cluster sizes of $n = 10, 14, 17$, the geometries appear equivalent to the best structures we have found. For $n = 16$, Shi et al. report not finding a structure lower in energy than either KJ or ASP, whereas we find a conformer lower in energy (by 2.24 and 0.48 kcal/mol for KJ and ASP respectively). For $n = 11$, Shi et al. agree with the ASP structure. For $n = 12, 15$, Shi et al.'s structures are topologically different from this work. We believe our structures are optimal at our level of theory, although we caution that global search methods cannot guarantee optimality. Paradoxically for $n = 13$, Shi et al. report that their structure is 0.46 kcal/mol *lower* in energy than KJ and 0.36 kcal/mol *higher* in energy than ASP, however with the level of theory used in this work we find both KJ and ASP to be nearly equal in energy (a 0.17 kcal/mol difference). This likely resulted from differences in the re-optimization of the KJ and ASP geometries. Examining the re-optimized KJ and ASP geometries of this work, they are found to be topologically equivalent to the starting geometries. As such, we assume Shi et al. optimized the KJ structure to a higher energy conformer. Therefore, we infer that the $n = 13$ conformer optimized in this work is lower in energy than the best structure given by Shi et al.[41]

General stability considerations

The general behavior of the energetics of the cluster growth can be seen in Figure 5, which compares our new data for protonated water clusters against the corresponding pure water clusters, as measured by interaction energy per water (E_I/n), and average hydrogen bond strength. Beginning with the protonated water clusters, the optimal structures for $n \leq 4$ represent the formation of the so-called "Eigen cation",[91] $H_3O^+(H_2O)_3$. The Eigen cation corresponds to hydrogen-bonding the 3 protons of hydronium ion with one water molecule each (see $n = 4$ in Figure 4). These hydrogen bonds are particularly strong,[92] as large

as 18 kcal/mol per hydrogen bond versus a water-water hydrogen bond of typically 3-5 kcal/mol. Beyond $n = 4$, the interaction energy per molecule weakens, as the Eigen cation interaction energy contribution is diluted. The E_I/n value appears to be on its way towards an asymptotic value from below, with a maximum value (i.e. smallest magnitude) of ~ -12 kcal/mol for the largest clusters considered here. Interestingly, the E_I/n curve for neutral water clusters also displays similar asymptotic behavior, albeit converging from above with a lowest value (i.e. largest magnitude) of ~ -8 kcal/mol at $n = 21$. (See reference 93 for a more detailed analysis of neutral water clusters.) Presumably these values for the protonated and neutral clusters will both eventually approach similar bulk water behavior. However on the size-scale of the clusters considered here, they are distinctly different, as shown in Figure 5.

For the protonated water clusters, $E_I/n_{\mathrm{H-bond}}$ values show a slow approach towards asymptotic behavior versus n in Figure 5, reaching a value of ~ 7 kcal/mol per hydrogen bond at $n = 21$. This contrasts with neutral water clusters which more rapidly approach ~ 5 kcal/mol beyond $n = 8$ as shown in Figure 5. The presence of the hydronium cation leads to strong cooperativity in the hydrogen bond network, which gradually weakens with cluster growth. The substructure visible in E_I/n_H with the values of $n = 7, 9, 12, 17$ showing weakened average hydrogen bond strengths does not connect to overall cluster stability because $n = 7, 9, 12, 17$ have an enhanced number of hydrogen bonds compared to their neighbors. It should also be noted that $n = 21$ shows no strong indication of special stability by these two measures.

Effective pairwise interactions: hydronium-water vs water-water

In order to examine the origins of the interaction energies in the cluster, the fourth-order effective 2-body interaction energies (as defined in reference 89) are used to disentangle the contributions from the hydronium-H_2O interactions and the H_2O-H_2O interactions. Figure 6 displays this breakdown as a function of cluster size. As can be seen, the hydronium-water

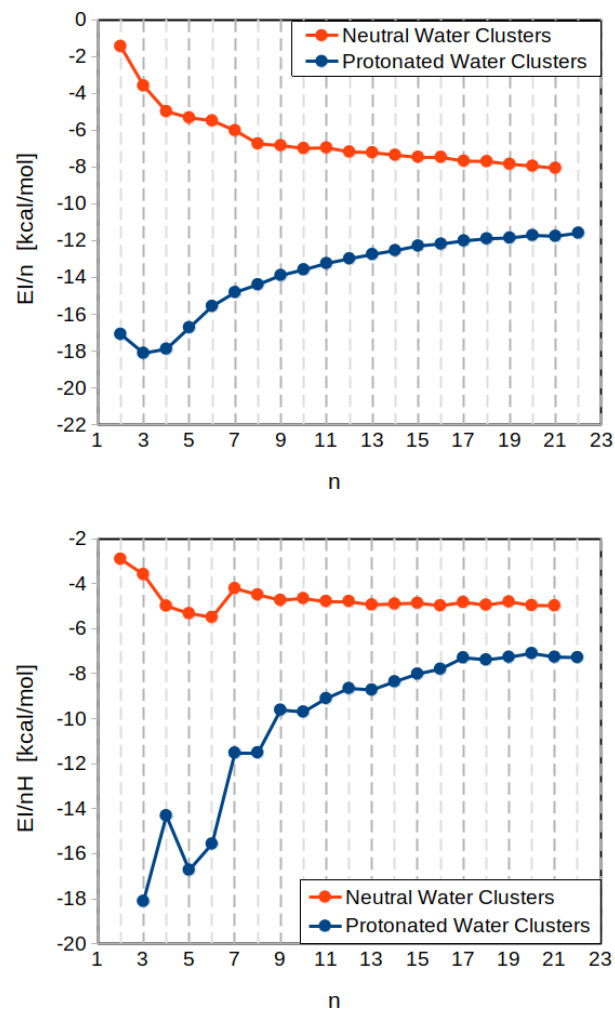Figure 5: The interaction energy per molecule (E_I/n) (top panel), and the average hydrogen bond strength (E_I/n_H) (bottom panel) as functions of cluster size for neutral water and protonated water. (ZPVE included.)

interactions dominate until $n = 16$, where there is a crossover and the H_2O-H_2O interaction energies begin to dominate. Additionally, the interplay between forming a strong hydrogen bond network versus maximization of the interaction energy with the hydronium ion can be seen as the cluster size increases; decreases in the hydronium-water interactions are mirrored by increases in water-water interaction energy, and vice versa.
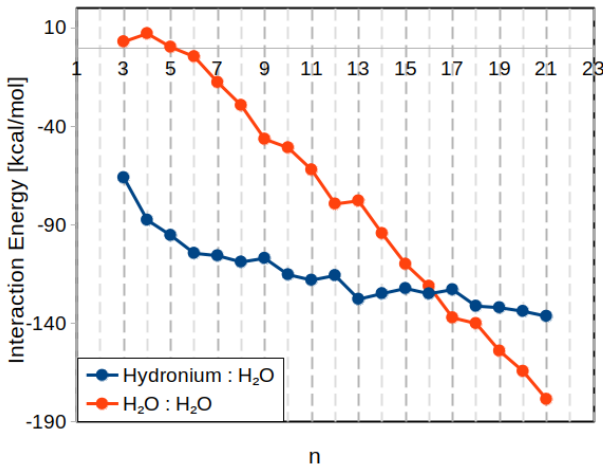

Figure 6: The sum of the effective 2-body interaction energies between the hydronium and H_2O molecules (blue), and between the H_2O molecules themselves in the global minimum structures of protonated water clusters. Note the crossover between $n = 16, 17$.

The size-dependent balance between hydronium-water and water-water interactions can be explained by a set of competing factors. The first factor is that the number of pairwise water-hydronium interactions increases linearly with cluster size, as $n - 1$, while the number of pairwise interactions within the H_2O network increases quadratically as $\frac{1}{2}(n-1)(n-2)$. The number of first solvent shell interactions is capped at 3 for hydronium-water, but grows roughly linearly with n for water-water interactions. The second factor is that once the three very strong hydronium-water hydrogen-bonds (~ 6 times as strong as the H_2O-H_2O interaction energies; see figure 7) of the Eigen cation are formed, subsequent second and higher solvent shell water interactions with hydronium ion become weaker. Therefore beyond $n = 4$, the increase in strength of interaction energy of the hydronium ion with the water molecules grows sub-linearly with n. The third factor is that hydronium-water interaction energies beyond the first solvent shell can remain as strong as a typical H_2O-H_2O hydrogen

24

bond even at distances of $\sim 6-7\text{Å}$. (Figure 7.) Strong intermediate-range hydronium water interactions reflect strong permanent (ion-dipole) electrostatics and (ion-induced dipole) polarization while dielectric screening of the ionic charge due to intervening water molecules is incomplete. Due to the small number of intervening molecules, this regime is far from bulk dielectric screening. Thus while the total interaction energy between the H_2O molecules continues to increase slightly super-linearly (see Figure 6), the point where water-water and hydronium-water interactions cross is only around $n = 16, 17$.
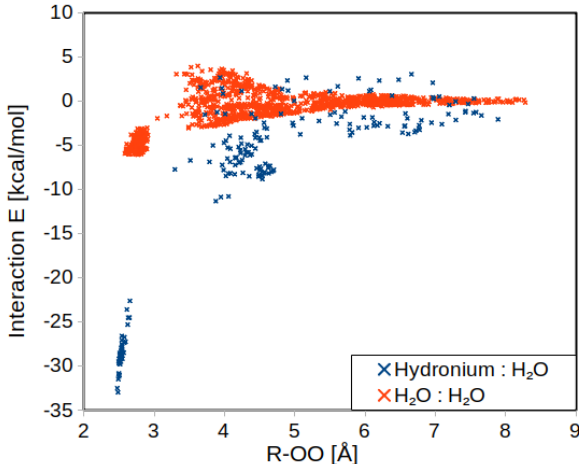

Figure 7: The effective 2-body interaction energies of hydronium-H_2O (blue) and H_2O-H_2O (orange) as a function of O-O distance, extracted from all cluster sizes.

Magic number considerations

Figure 8 displays the two main computational measures of special cluster stability as a function of cluster size: the sequential interaction energies (E_s; Eq. 3), and the second-order difference energies ($\Delta_2 E$; Eq. 5). For E_s, lower values represent higher energetic stability towards destruction as E_s measures single H_2O loss. For given n, a lower E_s compared to neighboring values (e.g. $n \pm 1$) can indicate a degree of special stability. For $\Delta_2 E$, both neighboring cluster sizes are considered, as such a cluster with a value less than zero is on average more energetically stable than its neighbors. For protonated water clusters, E_s and $\Delta_2 E$ are found to agree well with one another, with indications of special energetic

25

stability for cluster sizes with $n = 7, 9, 12, 14, 17, 19, 21$. Notably, beyond the Eigen cation formation in the very small clusters, $n = 21$ is the most stable cluster size found, agreeing with experimental findings.

We turn next to discussing the other specially stable cases identified above, and first note that the effects are generally subtle. The $n = 7$ cluster gains stability because it is the first cage closing, gaining some advantage over the open structure of $n = 6$ (see Figure 4). The lowest energy conformers of $n = 9, 12, 14, 16$ exhibit a characteristic structural feature wherein one of the H_2O molecules involved in the Eigen cation also acts as a hydrogen bond acceptor to an additional H_2O, as illustrated in Figure 9 (an "Eigen-aceptor"). The Eigen acceptor motif significantly *weakens* the affected hydronium-H_2O interaction (~ 24 kcal/mol compared to the average hydronium-H_2O hydrogen bond of ~ 28 kcal/mol). This indicates that the destabilization of the Eigen cation must be compensated for in a stronger water-water hydrogen bond network.

As one approaches bulk mixture, the hydronium ions will become fully solvated. Although there is no evidence for a non-surface hydronium ion in the lowest energy conformers for $n = 2 - 22$, these Eigen-acceptors may indicate a path to solvation. As the hydrogen bond network of the H_2O molecules becomes increasingly dominant, it may become more advantageous energetically to form these Eigen-acceptors (up to three per Eigen cation), even to the detriment of the stability of the Eigen cation itself.

Returning to the cluster stability question, the case of $n = 14$ can be explained by the fact that $n = 15$ represents the most unstable cluster in the hydronium dominated region (and second most unstable overall). This may contribute to the experimental observation of enhanced $n = 14$ signal. Cluster sizes of $n = 17, 19, 21$ appear to show special stability and also contain a fully coordinated ("core") H_2O (i.e. with 4 hydrogen bonds). However, as for the Eigen acceptor, it is unclear if this is the cause of the stability. The lowest energy conformer at $n = 16$ does not contain a core H_2O, yet has an E_s comparable to $n = 17$, and a slightly negative $\Delta_2 E$. Additionally, while $n = 18$ lacks a fully coordinated water and
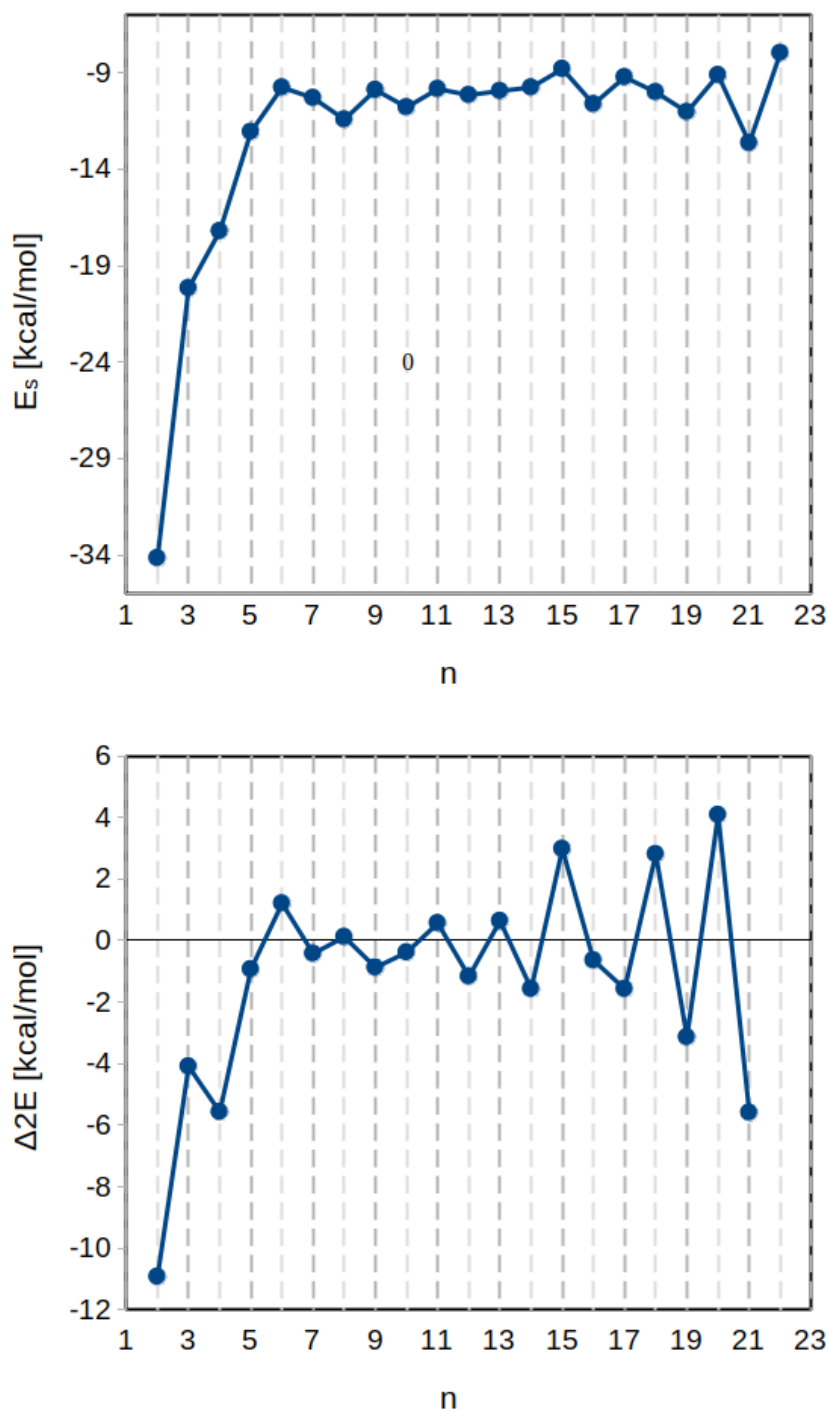
Figure 8: Calculated measures of "magic" of the lowest energy conformers of protonated water clusters. The upper panel shows the the sequential interaction energies, E_s (see Eq. 3), while the lower panel shows the second order difference energies, $\Delta_2 E$ (see Eq. 5). All plotted values include ZPVE.
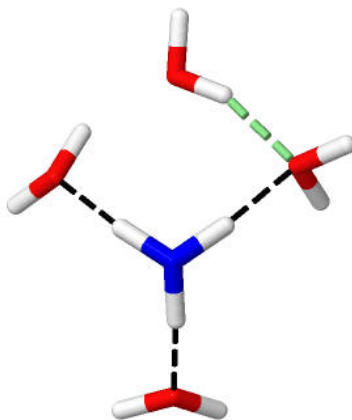
Figure 9: An illustration of the "Eigen-acceptor" hydrogen bond found in the lowest energy conformers of $n = 9, 12, 14$ and 16. This configuration destabilizes the hydronium-H_2O hydrogen bond by approximately 5 kcal/mol. This destabilization is compensated for elsewhere in the hydrogen bond network.

shows a high E_s and very positive $\Delta_2 E$, $n = 20$ *has* a core water and shows the highest E_s and most positive $\Delta_2 E$ of the full cluster size set.

Interestingly, as shown in Figure 10, this behavior of alternating core/non-core structures is observed in neutral water clusters, also beginning at n = 17; with the lowest energy conformers of n = 18, 20, and 24 not containing core H_2O.[93] Likewise, the fluctuations in E_s and $\Delta_2 E$ are more extreme across all cluster sizes for neutral water, whereas the extreme fluctuations for the protonated water clusters occur only beyond $n = 16$. This tendency for the larger protonated water clusters to mirror the neutral water cluster behavior is expected, given the crossover from hydronium dominated to H_2O dominated interaction energies as shown previously in Figure 6.

Conclusions

Our combined experimental and theoretical study of protonated water clusters provides insight into the interactions of the hydronium ion with the hydrogen bond network, and how this evolves as a function of size. Our main results and conclusions can be summarized as follows:
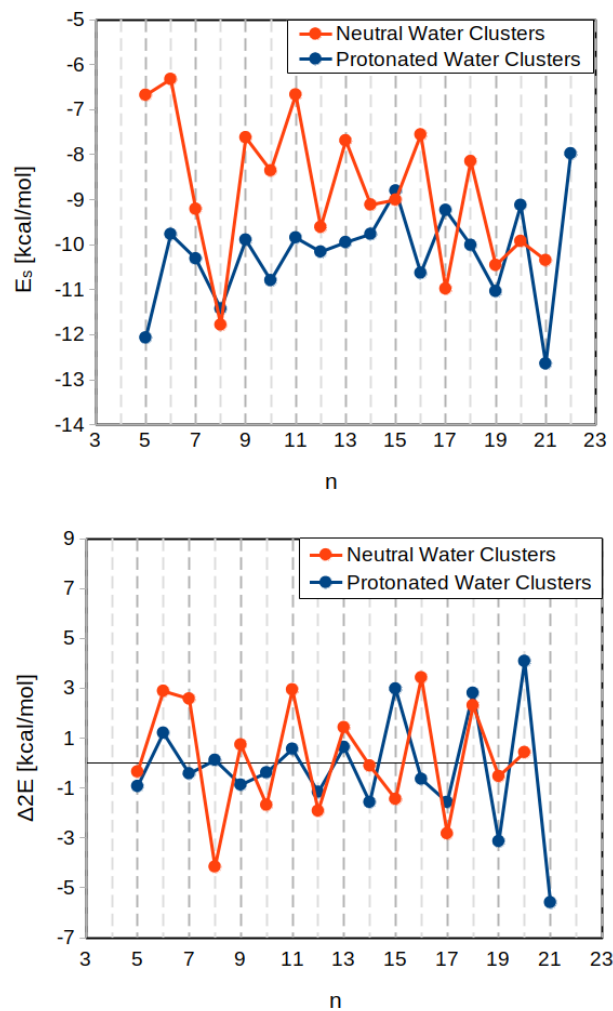
Figure 10: Top panel: The E_s of neutral water clusters (orange) compared to the E_s of protonated water clusters (blue). Bottom panel: The $\Delta_2 E$ of neutral water clusters (orange) compared to the $\Delta_2 E$ of protonated water clusters (blue). (ZPVE included.)

1. The experimental results show unequivocally that apart from $H^+(H_2O)_{21}$, a new magic number of $H^+(H_2O)_{14}$ is clearly observed especially at lower photon energies and shorter nozzle to ionization distances.

2. We have performed a careful computational search for the most stable conformer of protonated water clusters from $n = 2$ to $n = 22$, using metadynamics methods followed by refinement with DFT methods that are quite accurate for hydrogen-bonded systems. To the best of our knowledge, we have presented new lower energy structures for $n = 5, 6, 11, 12, 16, 18$. Our energies are ZPVE corrected, to represent zero temperature binding enthalpies.

3. Consistent with previous work, computational measures of cluster stability suggest that the $n = 21$ protonated cluster is particularly stable. Interestingly, the $n = 14$ cluster that is prominent experimentally emerges as stabilized relative to its neighbors at $n = 13$ and $n = 15$ as measured by its computed second order stabilization energy, which may contribute to its experimental observation. Other clusters with indications of special stability include $n = 12, 19$.

4. The computational results for protonated water clusters were analyzed in terms of effective two-body interactions which sum exactly to the total interaction energy. This analysis reveals a cross-over as a function of cluster size between a water-hydronium dominated regime for small clusters and a water-water dominated regime for larger clusters around n = 17. In the latter regime, protonated water clusters are similar to neutral water clusters with structure and energetics being dominated by the hydrogen bonding network.

5. The experimental observation of a prominent peak for $n = 14$, while qualitatively consistent with the computational calculations, cannot be attributed solely to special stability (e.g. $n = 19$ looks equally compelling). Rather, the different non-equilibrium

cluster distributions sampled by varying photon energies and nozzle distances are also clearly critical.

Supporting Information

Instructions for visualizing experimental mass spectra and photoionization intensity curves. Additional figures and optimized structures of conformers (SI.pdf)

Raw data

(raw_data_for_plots.xls; mass_spec_data.xls)

Conflicts of Interest

MHG is a part-owner of Q-Chem Inc, whose software was used for many of the calculations reported here.

Acknowledgement

References

(1) Ball, P. Water is an active matrix of life for cell and molecular biology. *Proc. Natl. Acad. Sci. USA* **2017**, *114*, 13327–13335.

(2) Vaida, V. Perspective: Water cluster mediated atmospheric chemistry. *J. Chem. Phys.* **2011**, *135*, 020901.

(3) Lu, W.; Mackie, C. J.; Xu, B.; Head-Gordon, M.; Ahmed, M. A Computational and Experimental View of Hydrogen Bonding in Glycerol Water Clusters. *J. Phys. Chem. A* **2022**,

(4) Ahmed, M.; Kostko, O. From atoms to aerosols: probing clusters and nanoparticles with synchrotron based mass spectrometry and X-ray spectroscopy. *Phys. Chem. Chem. Phys.* **2020**, *22*, 2713–2737.

(5) Searcy, J.-Q.; Fenn, J. Clustering of water on hydrated protons in a supersonic free jet expansion. *J. Chem. Phys.* **1974**, *61*, 5282–5288.

(6) Hansen, K.; Andersson, P. U.; Uggerud, E. Activation energies for evaporation from protonated and deprotonated water clusters from mass spectra. *J. Chem. Phys.* **2009**, *131*, 124303.

(7) Hansen, K.; Ryding, M.; Uggerud, E. Magic numbers and stabilities of heavy water clusters, (D2O)ND+, N = 3-48. *Int. J. Mass Spectrom.* **2019**, *440*, 14–19.

(8) Lengyel, J.; Pysanenko, A.; Poterya, V.; Kočišek, J.; Fárník, M. Extensive water cluster fragmentation after low energy electron ionization. *Chem. Phys. Lett.* **2014**, *612*, 256–261.

(9) Shin, J.-W.; Hammer, N.; Diken, E.; Johnson, M.; Walters, R.; Jaeger, T.; Duncan, M.; Christie, R.; Jordan, K. D. Infrared signature of structures associated with the H+ (H2O) n (n= 6 to 27) clusters. *Science* **2004**, *304*, 1137–1140.

(10) Miyazaki, M.; Fujii, A.; Ebata, T.; Mikami, N. Infrared spectroscopic evidence for protonated water clusters forming nanoscale cages. *Science* **2004**, *304*, 1134–1137.

(11) Headrick, J. M.; Diken, E. G.; Walters, R. S.; Hammer, N. I.; Christie, R. A.; Cui, J.; Myshakin, E. M.; Duncan, M. A.; Johnson, M. A.; Jordan, K. D. Spectral signatures of hydrated proton vibrations in water clusters. *Science* **2005**, *308*, 1765–1769.

(12) Li, G.; Zhang, Y.-Y.; Li, Q.; Wang, C.; Yu, Y.; Zhang, B.; Hu, H.-S.; Zhang, W.; Dai, D.; Wu, G. et al. Infrared spectroscopic study of hydrogen bonding topologies in the smallest ice cube. *Nat. Commun.* **2020**, *11*, 1–6.

(13) Jiang, S.; Su, M.; Yang, S.; Wang, C.; Huang, Q.-R.; Li, G.; Xie, H.; Yang, J.; Wu, G.; Zhang, W. et al. Vibrational Signature of Dynamic Coupling of a Strong Hydrogen Bond. *J. Phys. Chem. Lett.* **2021**, *12*, 2259–2265.

(14) Zhang, Y.-Y.; Wang, C.; Li, G.; Zang, X.; Yu, Y.; Hu, H.-S.; Yang, J.; Zhang, W.; Dai, D.; Wu, G. et al. Infrared spectroscopic signature of the structural diversity of the water heptamer. *Cell Rep. Phys. Sci.* **2022**, *3*, 100748.

(15) Buck, U.; Huisken, F. Infrared Spectroscopy of Size-Selected Water and Methanol Clusters. *Chem. Rev.* **2000**, *100*, 3863–3890, PMID: 11749332.

(16) Buck, U.; Pradzynski, C.; Zeuch, T.; Dieterich, J.; Hartke, B. A size-resolved perspective of large water clusters. *Phys. Chem. Chem. Phys.* **2014**, *16*, 6859–6871.

(17) Becker, D.; Dierking, C. W.; Suchan, J.; Zurheide, F.; Lengyel, J.; Fárník, M.; Slavíček, P.; Buck, U.; Zeuch, T. Temperature evolution in IR action spectroscopy experiments with sodium doped water clusters. *Phys. Chem. Chem. Phys.* **2021**, *23*, 7682–7695.

(18) Zeng, H. J.; Johnson, M. A. Demystifying the diffuse vibrational spectrum of aqueous protons through cold cluster spectroscopy. *Annu. Rev. Phys. Chem.* **2021**, *72*, 667–691.

(19) Jongma, R. T.; Huang, Y.; Shi, S.; Wodtke, A. M. Rapid evaporative cooling suppresses fragmentation in mass spectrometry: synthesis of "unprotonated" water cluster ions. *J. Phys. Chem. A* **1998**, *102*, 8847–8854.

(20) Dong, F.; Heinbuch, S.; Rocca, J. J.; Bernstein, E. R. Dynamics and fragmentation of van der Waals clusters:(H2O)n,(CH3OH)n, and (NH3)n upon ionization by a 26.5 eV soft x-ray laser. *J. Chem. Phys.* **2006**, *124*, 224319.

(21) Belau, L.; Wilson, K. R.; Leone, S. R.; Ahmed, M. Vacuum ultraviolet (VUV) photoionization of small water clusters. *J. Phys. Chem. A* **2007**, *111*, 10075–10083.

(22) Apicella, B.; Li, X.; Passaro, M.; Spinelli, N.; Wang, X. Multiphoton ionization of large water clusters. *J. Chem. Phys.* **2014**, *140*, 204313.

(23) Kočišek, J.; Lengyel, J.; Fárník, M.; Slavíček, P. Energy and charge transfer in ionized argon coated water clusters. *J. Chem. Phys.* **2013**, *139*, 214308.

(24) Huang, C.; Kresin, V. V.; Pysanenko, A.; Fárník, M. Water cluster fragmentation probed by pickup experiments. *J. Chem. Phys.* **2016**, *145*, 104304.

(25) Golan, A.; Ahmed, M. Ionization of water clusters mediated by exciton energy transfer from argon clusters. *J. Phys. Chem. Lett.* **2012**, *3*, 458–462.

(26) Mizuse, K.; Kuo, J.-L.; Fujii, A. Structural trends of ionized water networks: Infrared spectroscopy of water cluster radical cations (H2O) n+ (n= 3–11). *Chem. Sci.* **2011**, *2*, 868–876.

(27) Kochanski, E.; Kelterbaum, R.; Klein, S.; Rohmer, M.; Rahmouni, A. Decades of theoretical work on protonated hydrates. In *Adv. Quantum Chem.*; Elsevier, 1997; Vol. 28; pp 273–291.

(28) Chang, H.-C.; Wu, C.-C.; Kuo, J.-L. Recent advances in understanding the structures of medium-sized protonated water clusters. *Int. Rev. Phys. Chem.* **2005**, *24*, 553–578.

(29) Shi, R.; Huang, X.; Su, Y.; Lu, H.-G.; Li, S.-D.; Tang, L.; Zhao, J. Which density functional should be used to describe protonated water clusters? *J. Phys. Chem. A* **2017**, *121*, 3117–3127.

(30) Heindel, J. P.; Yu, Q.; Bowman, J. M.; Xantheas, S. S. Benchmark electronic structure calculations for H3O+ (H2O) n, n= 0–5, clusters and tests of an existing 1, 2, 3-body potential energy surface with a new 4-body correction. *J. Chem. Theory Comput.* **2018**, *14*, 4553–4566.

(31) Egan, C. K.; Paesani, F. Assessing many-body effects of water self-ions. II: H3O+ (H2O) n clusters. *J. Chem. Theory Comput.* **2019**, *15*, 4816–4833.

(32) Kulig, W.; Agmon, N. Deciphering the infrared spectrum of the protonated water pentamer and the hybrid Eigen–Zundel cation. *Phys. Chem. Chem. Phys.* **2014**, *16*, 4933–4941.

(33) Fagiani, M. R.; Knorke, H.; Esser, T. K.; Heine, N.; Wolke, C. T.; Gewinner, S.; Schöllkopf, W.; Gaigeot, M.-P.; Spezia, R.; Johnson, M. A. et al. Gas phase vibrational spectroscopy of the protonated water pentamer: the role of isomers and nuclear quantum effects. *Phys. Chem. Chem. Phys.* **2016**, *18*, 26743–26754.

(34) Mella, M.; Kuo, J.-L.; Clary, D. C.; Klein, M. L. Nuclear quantum effects on the structure and energetics of (H2O)6H+. *Phys. Chem. Chem. Phys.* **2005**, *7*, 2324–2332.

(35) Heine, N.; Fagiani, M. R.; Rossi, M.; Wende, T.; Berden, G.; Blum, V.; Asmis, K. R. Isomer-selective detection of hydrogen-bond vibrations in the protonated water hexamer. *J. Am. Chem. Soc.* **2013**, *135*, 8266–8273.

(36) Jiang, J.-C.; Wang, Y.-S.; Chang, H.-C.; Lin, S. H.; Lee, Y. T.; Niedner-Schatteburg, G.; Chang, H.-C. Infrared spectra of H+ (H2O) 5-8 clusters: Evidence for symmetric proton hydration. *J. Am. Chem. Soc.* **2000**, *122*, 1398–1410.

(37) Lin, C.-K.; Wu, C.-C.; Wang, Y.-S.; Lee, Y. T.; Chang, H.-C.; Kuo, J.-L.; Klein, M. L. Vibrational predissociation spectra and hydrogen-bond topologies of H+(H 2 O) 9–11. *Phys. Chem. Chem. Phys.* **2005**, *7*, 938–944.

(38) Schran, C.; Brieuc, F.; Marx, D. Transferability of machine learning potentials: Protonated water neural network potential applied to the protonated water hexamer. *J. Chem. Phys.* **2021**, *154*, 051101.

(39) Hodges, M. P.; Wales, D. J. Global minima of protonated water clusters. *Chem. Phys. Lett.* **2000**, *324*, 279–288.

(40) James, T.; Wales, D. J.; Hernández-Rojas, J. Global minima for water clusters (H2O) n, n≤21, described by a five-site empirical potential. *Chem. Phys. Lett.* **2005**, *415*, 302–307.

(41) Shi, R.; Li, K.; Su, Y.; Tang, L.; Huang, X.; Sai, L.; Zhao, J. Revisit the landscape of protonated water clusters H+ (H2O) n with n= 10–17: An ab initio global search. *J. Chem. Phys.* **2018**, *148*, 174305.

(42) Kozack, R.; Jordan, P. Empirical models for the hydration of protons. *J. Chem. Phys.* **1992**, *96*, 3131–3136.

(43) Hodges, M. P.; Stone, A. J. Modeling small hydronium–water clusters. *J. Chem. Phys.* **1999**, *110*, 6766–6772.

(44) Zhao, J.; Shi, R.; Sai, L.; Huang, X.; Su, Y. Comprehensive genetic algorithm for ab initio global optimisation of clusters. *Mol. Sim.* **2016**, *42*, 809–819.

(45) Iyengar, S. S.; Petersen, M. K.; Day, T. J.; Burnham, C. J.; Teige, V. E.; Voth, G. A. The properties of ion-water clusters. I. The protonated 21-water cluster. *J. Chem. Phys.* **2005**, *123*, 084309.

(46) Torrent-Sucarrat, M.; Anglada, J. M. Anharmonicity and the Eigen-Zundel dilemma in the IR spectrum of the protonated 21 water cluster. *J. Chem. Theory Comput.* **2011**, *7*, 467–472.

(47) Liu, J.; Yang, J.; Zeng, X. C.; Xantheas, S. S.; Yagi, K.; He, X. Towards complete assignment of the infrared spectrum of the protonated water cluster H+ (H2O) 21. *Nat. Commun.* **2021**, *12*, 1–10.

(48) Zwier, T. S. The structure of protonated water clusters. *Science* **2004**, *304*, 1119–1120.

(49) Hagena, O. F. Cluster ion sources. *Rev. Sci. Instrum.* **1992**, *63*, 2374–2379.

(50) Hagena, O.; Obert, W. Cluster formation in expanding supersonic jets: Effect of pressure, temperature, nozzle size, and test gas. *J. Chem. Phys.* **1972**, *56*, 1793–1802.

(51) Bandyopadhyay, B.; Cheng, T.; Duncan, M. Proton sharing in hydronium–nitrogen clusters probed with infrared spectroscopy. *Int. J. Mass Spectrom.* **2010**, *297*, 124–130.

(52) Douberly, G. E.; Ricks, A. M.; Ticknor, B. W.; McKee, W. C.; Schleyer, P. v. R.; Duncan, M. A. Infrared photodissociation spectroscopy of protonated acetylene and its clusters. *J. Phys. Chem. A* **2008**, *112*, 1897–1906.

(53) Duncan, M. A. Invited review article: laser vaporization cluster sources. *Rev. Sci. Instrum.* **2012**, *83*, 041101.

(54) Relph, R. A.; Bopp, J. C.; Roscioli, J. R.; Johnson, M. A. Structural characterization of (C 2 H 2) 1–6+ cluster ions by vibrational predissociation spectroscopy. *J. Chem. Phys.* **2009**, *131*, 114305.

(55) Bandyopadhyay, B.; Kostko, O.; Fang, Y.; Ahmed, M. Probing methanol cluster growth by vacuum ultraviolet ionization. *J. Phys. Chem. A* **2015**, *119*, 4083–4092.

(56) Bandyopadhyay, B.; Stein, T.; Fang, Y.; Kostko, O.; White, A.; Head-Gordon, M.; Ahmed, M. Probing ionic complexes of ethylene and acetylene with vacuum-ultraviolet radiation. *J. Phys. Chem. A* **2016**, *120*, 5053–5064.

(57) Stein, T.; Bandyopadhyay, B.; Troy, T. P.; Fang, Y.; Kostko, O.; Ahmed, M.; Head-Gordon, M. Ab initio dynamics and photoionization mass spectrometry reveal ion–molecule pathways from ionized acetylene clusters to benzene cation. *Proc. Natl. Acad. Sci. USA* **2017**, *114*, E4125–E4133.

(58) Wilson, K. R.; Jimenez-Cruz, M.; Nicolas, C.; Belau, L.; Leone, S. R.; Ahmed, M. Thermal Vaporization of Biological Nanoparticles: Fragment-Free Vacuum Ultraviolet Photoionization Mass Spectra of Tryptophan, Phenylalanine-Glycine-Glycine, and β-Carotene. *J. Phys. Chem. A* **2006**, *110*, 2106–2113.

(59) Kamarchik, E.; Kostko, O.; Bowman, J. M.; Ahmed, M.; Krylov, A. I. Spectroscopic signatures of proton transfer dynamics in the water dimer cation. *J. Chem. Phys.* **2010**, *132*, 194311.

(60) Marsalek, O.; Elles, C. G.; Pieniazek, P. A.; Pluhařová, E.; VandeVondele, J.; Bradforth, S. E.; Jungwirth, P. Chasing charge localization and chemical reactivity following photoionization in liquid water. *J. Chem. Phys.* **2011**, *135*, 224510.

(61) Svoboda, O.; Hollas, D.; Ončák, M.; Slavíček, P. Reaction selectivity in an ionized water dimer: nonadiabatic ab initio dynamics simulations. *Phys. Chem. Chem. Phys.* **2013**, *15*, 11531–11542.

(62) Mardirossian, N.; Head-Gordon, M. ω B97M-V: A combinatorially optimized, range-separated hybrid, meta-GGA density functional with VV10 nonlocal correlation. *J. Chem. Phys.* **2016**, *144*, 214110.

(63) Mardirossian, N.; Head-Gordon, M. Thirty years of density functional theory in com-

putational chemistry: An overview and extensive assessment of 200 density functionals. *Mol. Phys.* **2017**, *115*, 2315–2372.

(64) Najibi, A.; Goerigk, L. The nonlocal kernel in van der Waals density functionals as an additive correction: An extensive analysis with special emphasis on the B97M-V and ωB97M-V approaches. *J. Chem. Theory Comput.* **2018**, *14*, 5725–5738.

(65) Liang, J.; Feng, X.; Liu, X.; Head-Gordon, M. Analytical harmonic vibrational frequencies with VV10-containing density functionals: Theory, efficient implementation, and benchmark assessments. *J. Chem. Phys.* **2023**, *158*, 204109.

(66) Pracht, P.; Bohle, F.; Grimme, S. Automated exploration of the low-energy chemical space with fast quantum chemical methods. *Phys. Chem. Chem. Phys.* **2020**, *22*, 7169–7192.

(67) Grimme, S. Exploration of chemical compound, conformer, and reaction space with meta-dynamics simulations based on tight-binding quantum chemical calculations. *J. Chem. Theory Comput.* **2019**, *15*, 2847–2862.

(68) Wales, D. J.; Doye, J. P. Global optimization by basin-hopping and the lowest energy structures of Lennard-Jones clusters containing up to 110 atoms. *J. Phys. Chem. A* **1997**, *101*, 5111–5116.

(69) Do, H.; Besley, N. A. Structural optimization of molecular clusters with density functional theory combined with basin hopping. *J. Chem. Phys.* **2012**, *137*, 134106.

(70) Bannwarth, C.; Ehlert, S.; Grimme, S. GFN2-xTB—An accurate and broadly parametrized self-consistent tight-binding quantum chemical method with multipole electrostatics and density-dependent dispersion contributions. *J. Chem. Theory Comput.* **2019**, *15*, 1652–1671.

(71) Epifanovsky, E.; Gilbert, A. T.; Feng, X.; Lee, J.; Mao, Y.; Mardirossian, N.; Pokhilko, P.; White, A. F.; Coons, M. P.; Dempwolff, A. L. et al. Software for the frontiers of quantum chemistry: An overview of developments in the Q-Chem 5 package. *J. Chem. Phys.* **2021**, *155*, 084801.

(72) Vydrov, O. A.; Van Voorhis, T. Nonlocal van der Waals density functional: The simpler the better. *J. Chem. Phys.* **2010**, *133*, 244103.

(73) Mardirossian, N.; Head-Gordon, M. ωB97X-V: A 10-parameter, range-separated hybrid, generalized gradient approximation density functional with nonlocal correlation, designed by a survival-of-the-fittest strategy. *Phys. Chem. Chem. Phys.* **2014**, *16*, 9904–9924.

(74) Weigend, F.; Ahlrichs, R. Balanced basis sets of split valence, triple zeta valence and quadruple zeta valence quality for H to Rn: Design and assessment of accuracy. *Phys. Chem. Chem. Phys.* **2005**, *7*, 3297–3305.

(75) Rappoport, D.; Furche, F. Property-optimized Gaussian basis sets for molecular response calculations. *J. Chem. Phys.* **2010**, *133*, 134105.

(76) Fink, R. F. Why does MP2 work? *J. Chem. Phys.* **2016**, *145*, 184101.

(77) Fanourgakis, G. S.; Apra, E.; Xantheas, S. S. High-level ab initio calculations for the four low-lying families of minima of (H 2 O) 20. I. Estimates of MP2/CBS binding energies and comparison with empirical potentials. *J. Chem. Phys.* **2004**, *121*, 2655–2663.

(78) Yoo, S.; Apra, E.; Zeng, X. C.; Xantheas, S. S. High-level ab initio electronic structure calculations of water clusters (H2O) 16 and (H2O) 17: A new global minimum for (H2O) 16. *J. Phys. Chem. Lett.* **2010**, *1*, 3122–3127.

(79) Rakshit, A.; Bandyopadhyay, P.; Heindel, J. P.; Xantheas, S. S. Atlas of putative minima and low-lying energy networks of water clusters n= 3–25. *J. Chem. Phys.* **2019**, *151*, 214307.

(80) Lao, K. U.; Schäffer, R.; Jansen, G.; Herbert, J. M. Accurate description of intermolecular interactions involving ions using symmetry-adapted perturbation theory. *J. Chem. Theory Comput.* **2015**, *11*, 2473–2486.

(81) Lao, K. U.; Herbert, J. M. A simple correction for nonadditive dispersion within extended symmetry-adapted perturbation theory (XSAPT). *J. Chem. Theory Comput.* **2018**, *14*, 5128–5142.

(82) Shee, J.; Loipersberger, M.; Rettig, A.; Lee, J.; Head-Gordon, M. Regularized second-order Møller–Plesset theory: A more accurate alternative to conventional MP2 for non-covalent interactions and transition metal thermochemistry for the same computational cost. *J. Phys. Chem. Lett.* **2021**, *12*, 12084–12097.

(83) Xantheas, S. S. Ab-Initio Studies of Cyclic Water Clusters (H2O)(N), N=1-6 .2. Analysis of Many-Body Interactions. *J. Chem. Phys.* **1994**, *100*, 7523–7534.

(84) Xantheas, S. S. Cooperativity and hydrogen bonding network in water clusters. *Chem. Phys.* **2000**, *258*, 225–231.

(85) Cui, J.; Liu, H. B.; Jordan, K. D. Theoretical characterization of the (H2O)(21) cluster: Application of an n-body decomposition procedure. *J. Phys. Chem. B* **2006**, *110*, 18872–18878.

(86) Góra, U.; Podeszwa, R.; Cencek, W.; Szalewicz, K. Interaction energies of large clusters from many-body expansion. *J. Chem. Phys.* **2011**, *135*, 224102.

(87) Cobar, E. A.; Horn, P. R.; Bergman, R. G.; Head-Gordon, M. Examination of the hydrogen-bonding networks in small water clusters (n=2-5, 13, 17) using absolutely

localized molecular orbital energy decomposition analysis. *Phys. Chem. Chem. Phys.* **2012**, *14*, 15328–15339.

(88) Heindel, J. P.; Xantheas, S. S. The Many-Body Expansion for Aqueous Systems Revisited: I. Water-Water Interactions. *J. Chem. Theory Comput.* **2020**, *16*, 6843–6855.

(89) Mackie, C. J.; Zech, A.; Head-Gordon, M. Effective Two-Body Interactions. *J. Phys. Chem. A* **2021**, *125*, 7750–7758.

(90) Miller, D. R. Free jet sources. In *Atomic and molecular beam methods (Volume 1)*; Scoles, G., Ed.; Oxford University Press, Oxford, 1988; Chapter 2, pp 14–53.

(91) Eigen, M.; De Maeyer, L. Self-dissociation and protonic charge transport in water and ice. *Proc. Roy. Soc. London A* **1958**, *247*, 505–533.

(92) Parthasarathi, R.; Subramanian, V.; Sathyamurthy, N. Hydrogen bonding in protonated water clusters: an atoms-in-molecules perspective. *J. Phys. Chem. A* **2007**, *111*, 13287–13290.

(93) Liu, X.; Lu, W.-C.; Wang, C.; Ho, K. Energetic and fragmentation stability of water clusters (H2O) n, n= 2–30. *Chem. Phys. Lett.* **2011**, *508*, 270–275.

TOC Graphic